جامعة الملك عبدالله
للعلوم والتقنية
King Abdullah University of
Science and Technology

Effect of localized hydrodynamics on biofilm attachment and growth in a cross-flow filtration channel

Item Type	Article
Authors	Kerdi, Sarah;Qamar, Adnan;Vrouwenvelder, Johannes S.;Ghaffour, NorEddine
Citation	Kerdi, S., Qamar, A., Vrouwenvelder, J. S., & Ghaffour, N. (2020). Effect of localized hydrodynamics on biofilm attachment and growth in a cross-flow filtration channel. Water Research, 116502. doi:10.1016/j.watres.2020.116502
Eprint version	Post-print
DOI	10.1016/j.watres.2020.116502
Publisher	Elsevier BV
Journal	Water Research
Rights	NOTICE: this is the author's version of a work that was accepted for publication in Water Research. Changes resulting from the publishing process, such as peer review, editing, corrections, structural formatting, and other quality control mechanisms may not be reflected in this document. Changes may have been made to this work since it was submitted for publication. A definitive version was subsequently published in Water Research, [, , (2020-10-07)] DOI: 10.1016/j.watres.2020.116502 . © 2020. This manuscript version is made available under the CC-BY-NC-ND 4.0 license http://creativecommons.org/licenses/by-nc-nd/4.0/
Download date	2024-04-16 15:02:59
Link to Item	http://hdl.handle.net/10754/665490

Highlights

- Mapping of biofouling with hydrodynamics in filtration process.
- Pillar spacers with different filament diameters are studied.
- Bacterial attachment and growth on spacer and membrane are investigated.
- Thin spacer filament diameter revealed low attachment and fast biofilm growth on membrane.
- Thick spacer filament exhibited high attachment and slow biofilm growth on membrane.

Journal Pre-proof

Journal Pre-proof

Effect of localized hydrodynamics on biofilm attachment and growth in a cross-flow filtration channel

Sarah Kerdi, Adnan Qamar, Johannes S. Vrouwenvelder, Noreddine Ghaffour

King Abdullah University of Science and Technology (KAUST), Water Desalination and Reuse Center (WDRC), Biological and Environmental Science and Engineering (BESE), Thuwal 23955-6900, Saudi Arabia, Email: noreddine.ghaffour@kaust.edu.sa

Abstract

Biofilm attachment and growth in membrane filtration systems are considerably influenced by the localized flow inside the feed channel. The present work aims to map the biofilm attachment/growth mechanism under varying flow conditions. Effect of varying clearance region (space between the spacer filament and membrane surface) on biofouling pattern is investigated by using three 3D-printed pillar spacers having different filament diameters of 340, 500, and 1000 µm while maintaining the same pillar orientation, diameter and height. Direct Numerical Simulations (DNS) and Optical Coherence Tomography (OCT) were carried out to accurately predict the local hydrodynamics behavior and *in-situ* monitor the biofilm formation. On spacer filaments, biofouling attachment is primarily observed in the regions where low and non-fluctuating shear stresses are present. Conversely, on membrane surface, highest biofouling attachment was observed under spacer filaments where high shear stresses are prevalent along with low clearance height. Furthermore, as filtration time progresses, the biofilm grows faster on the membrane in the center of spacer cells where low shear stress with steady hydrodynamics conditions are prevalent. The proposed hydrodynamics approach envisages a full spectrum of spacer design constraints that can lead to intrinsic biofilm mitigation while improving filtration performance of membranes based water treatment.

Keywords: Hydrodynamics; Biofouling; 3D-printing; Shear stress; Filtration; Feed spacer filament diameter.

Journal Pre-proof

1. Introduction

Membrane filtration technologies are extensively utilized for water treatment and desalination purposes for extracting clean, fresh water. They tend to remove dissolved or suspended particulate compounds (biological, organic, and inorganic) from the feed solution. The membrane sheets used inside spiral wound modules are separated and supported by feed and permeate spacers (Schwinge et al., 2004a). Apart from membrane support, feed spacers are known to produce flow perturbation that has the potential to minimize concentration polarization, thereby enhancing permeate flux production (Schwinge et al., 2004b; Schwinge et al., 2000). However, these spacers introduce pressure drop into the channel that effectively tarnishes the energy requirements, especially when the membrane is fouled (Ali et al., 2019; Hijnen et al., 2009). In biological active feed solutions, these spacers intensify biofouling (a protective matrix for microorganisms, produced through accumulation of biomass and excretion of extracellular polymeric substances (EPS) in favorable conditions), which presents a major challenge in filtration operations (Huang et al., 2010).

In water treatment processes, the biofilm formation on the membrane surface occurs due to microbial adhesion and growth. This, in turn, depends on surface characteristics of the membrane and feed spacer such as hydrophobicity, roughness, zeta potential, surface energy (Bernstein et al., 2011; Habimana et al., 2014; Kang and Choi, 2005; Subramani and Hoek, 2008) and on the intrinsic features of microorganisms (Pang et al., 2005; Vrijenhoek et al., 2001). Moreover, hydrodynamics in the filtration microchannel (fluid shear stress) plays a vital role in microbial adhesion and growth (Rickard et al., 2004; Ying et al., 2013). In a cross-flow filtration setup, the bacteria and nutrients are directed towards the membrane surface by feed spacer filaments (generally circular

Journal Pre-proof

cross-sections). Therefore, adhesion tendency is higher when spacers are presented (Huang et al., 2010).

The hydrodynamics shear stress has an ambivalent influence on biofilm attachment (at the early stage of biofouling) and growth (at the mature stage of biofouling) mechanisms. In biological studies on a substratum, where hydrodynamics is steady in nature, a low surface shear stress limits the biofilm detachment and potentially promotes biofilm development (Liu and Tay, 2002; Shen et al., 2015). On the other hand, the high shear on substratum can facilitate more access to bacteria and dissolved nutrients to the surface. It has been reported that high shear on a substratum results in an initial stronger and faster bacterial adhesion (Roosjen et al., 2005; Siddiqui et al., 2019) and the least biofilm growth (Radu et al., 2010). However, this situation is reversed in unsteady/turbulent flows. An excessive perturbed flow is associated with higher fluctuating membrane shear stresses, averting extensive bacterial growth (Perni et al., 2006; Purevdorj et al., 2002).

From several decades, the commercial feed spacer design and geometry mostly remain the same. It usually comprises of a non-woven pattern having variable circular cross-section filaments. Many experimental studies have focused on optimizing spacer design and/or coatings while monitoring the biofilm growth to evaluate the pressure drop and Sherwood correlations (Araújo et al., 2012; Da Costa et al., 1991; Koutsou et al., 2009; Schock and Miquel, 1987; Siddiqui et al., 2017; Zimmerer and Kottke, 1996). Few computational hydrodynamics studies aimed to study particle deposition in spacer filled channels, with limited highlights on attachment/growth models (Li et al., 2012; Radu et al., 2014). X-ray computed tomography has provided insight in the spacer geometries (Haaksman et al., 2017). However, compared to experimental observations, numerical results were well correlated for particulate fouling (Radu et al., 2014).

For the commercial spacers which have varying filament cross-sections, the local hydrodynamics is complex and strongly influenced by the incoming feed flow velocity (or channel's Reynolds number). As such, based on the clearance region (free space) between the spacer filament and the membrane surface, it produces local spatial variations in velocity magnitude and shear stress, which can be under steady or unsteady flow environment. Given the intricate nature of spacer design and associated hydrodynamics, it is challenging to design experiments where biofilm correlation with hydrodynamics conditions (local fluid shear and velocity) and geometrical parameters (varying clearance region height) can be achieved. In fact, to date, accurate hydrodynamics prediction on realistic commercial geometries is still hard to perform when the flow is unsteady as it required considerable computational resources (Qamar et al., 2019). Thus, for efficient filtration, a clear and deep understanding of local hydrodynamics on biofilm adhesion and growth in a filtration channel filled by feed spacer is still currently vague and lacks scientific insights.

The present work aims to highlight the role of local hydrodynamics and geometric clearance on biofilm adhesion and growth inside a spacer filled filtration channel. To simplify the associated complexity of commercial spacer design (non-uniform diameter along the length of the filament due to the manufacturing process), recently proposed column spacers (Ali et al., 2019) are used in this study. The merit of this spacer design is that filaments are symmetric (non-woven and located centrally), and cross-section areas along the length of the filaments are constant, which gives uniform control on the clearance region and fluid shear stress/velocity distributions. Three spacer configurations having different filament diameters are experimentally operated in a lab-scale ultrafiltration (UF) setup under varying operating conditions. Biofouling development is *in-situ* visualized by using optical coherence tomography (OCT) (Kerdi et al., 2019). To gain

full insight into the hydrodynamics, direct numerical simulations (DNS) are also performed for each operating condition using the exact designs of pillar spacers. A strong correlation between spatial hydrodynamics conditions (steady/unsteady, fluid shear stress) and biofilm attachment and growth is observed. The present work aims to propose a novel approach to enhance fundamental understanding between hydrodynamics and associate biofilm growth and performance in UF systems which constitute the crucial stage of pretreatment for nanofiltration (NF) and reverse osmosis (RO) in the industrial implementation. In addition, this study provides an impetus and clear-cut guidance to feed spacer designers with an additional parameter to control biofouling apart from pressure drop minimization and permeate flux enhancement. The correlation of fluid shear stress with biofilm growth is thus pivotal to design new spacers/channel configuration in an attempt to self-mitigate biofouling intrinsically.

2. Materials and methods

This section outlines the feed spacer characteristics and the experimental protocol utilized to achieve the lab-scale filtration tests. The flow parameters and numerical approach used in the present work are as well highlighted in this section.

2.1. Feed spacer design

Three different pillar spacers, having the same pillar orientation, diameter (D_p = 1000 µm) and height (H = 1200 µm) were in-house manufactured via UV polymerization of acrylate monomer (liquid resin, BV007) by 3D printing technology (MIICRAFT 125, Version 3.4.5, MiiCraft Inc.). Similar design of feed spacer (D_p = 1500 µm, H = 1200 µm and a fixed filament diameter of 500 µm) is utilized by Syed et al. (Ali et al., 2019) to evaluate UF performance in a cross-flow system. The thickness of the spacers is kept as H = 1200 µm owing to limitations

arising from 3D printing, which is also seen in earlier research work (Ali et al., 2019) pertaining to 3D printing of feed spacers. From application perspective, usually the spacer thickness is below 1000 µm. However, results either generated through current work or previous studies can be scaled down using scaling arguments for interpretation at smaller scales. In present work, the printed pillar spacers were distinguished by different filament diameters to study their impact on hydrodynamics conditions and biofouling phenomena. The tested filament diameters (D_F) are 340 µm, 500 µm and 1000 µm for pillar spacers denoted by P-340, P-500, and P-1000, respectively. The resulted clearance region heights (h), as well as the porosities of the various spacer-filled feed channels are depicted in Table 1.

2.2. Experimental protocol

As we aim to study the effect on biofouling under varying hydrodynamics conditions, UF system was considered suitable for the study as most pretreatment systems, like UF, often encounters sever biofouling in desalination plants. The lab-scale UF setup and various instruments used for the filtration tests are depicted in Figure 1. By varying the operating conditions (Table 1), two sets of UF experiments were conducted for all three spacers for a period of 67 h. For each set, three identical flow cells were simultaneously utilized in a cross-flow filtration mode. They have a filtration area of 60 mm × 15 mm and a filtration feed channel of 1.2 mm as height. Coupons of UF membrane (STERLITECH, Synder flat sheet membrane, polyethersulfone, MWCO of 100 kDa) and feed spacer were installed in the filtration channel of each flow cell. The feed solution was continuously stirred throughout the filtration tests with a magnetic stirrer (IKA, model RCTBS002) at 200 RPM and was pumped to the filtration modules by three gear pumps (COLE-PARMER, model 75211-70). In order to monitor the applied feed pressure on the filtration module (P ~ 1 bar), two gauge pressures (ASHCROFT, model 1005)

were placed at the inlet and outlet of each flow cell. The adjustment of the volumetric flow rate (Q) inside the flow cell was controlled by a valve connected to a flowmeter (DWYER, model RMB-SSV) placed both at the outlet of each filtration line. A data acquisition system (National Instruments, LabView, 2016) was used to continuously record the weight of collected permeate fluxes read by electronic balances (METTLER TOLEDO, MS3002S). The visualization of biofouling attached and developed on the spacer and membrane surfaces was achieved by Optical Coherence Tomography (OCT) (THORLABS, Hyperion) at 12 and 67 h of filtration process. The two-dimensional scanned images were post-processed through *ImageJ* software (U. S. National Institutes of Health, USA). Channel pressure drop measurements (ΔP) were separately performed by using a differential pressure transmitter (OMEGA, model PX5200 M5091/0112).

Journal Pre-proof

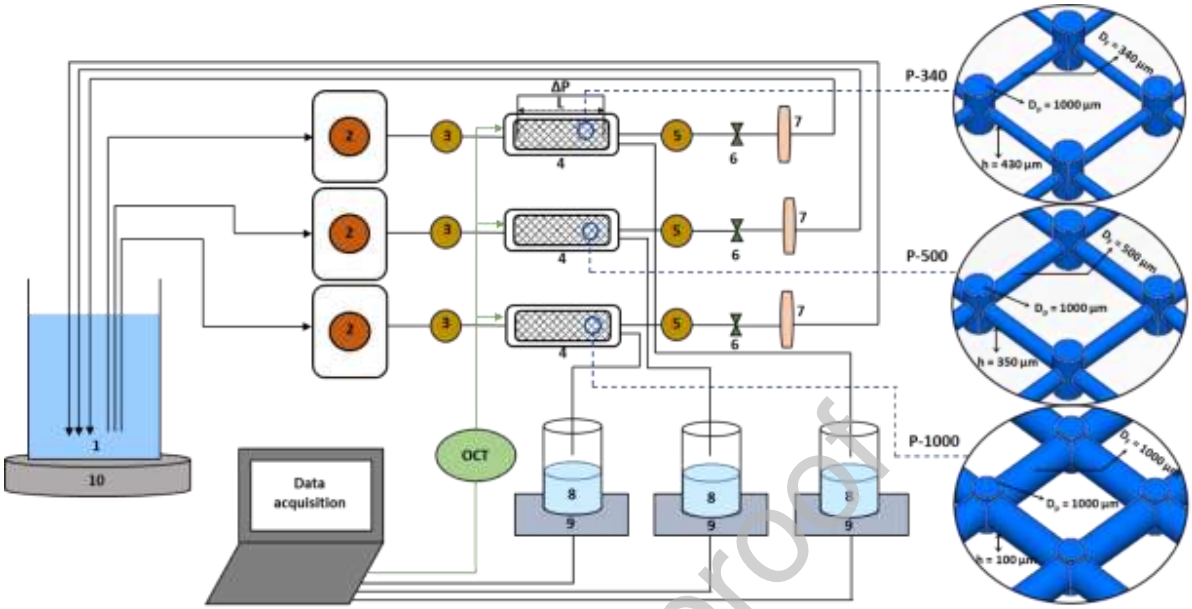

1: Feed solution tank, 2: Gear Pumps, 3: Inlet gauge pressure ($P_3 \approx 1$ bar), 4: Flow cell modules (spacer, UF membrane), 5: Outlet gauge pressure ($P_5 \approx 1$ bar), 6: Valves, 7: Flowmeters, 8: Permeate collection tanks, 9: Balances, 10: Magnetic stirrer. ΔP is the differential value of pressures measured inside the channel through pressure probes placed at a distance L.

Fig. 1. Schematic of lab-scale setup along with various types of equipment used in UF experimental tests. Inserted on right the top view of various pillar spacers (P-340, P-500 and P-1000) used in three flow cell modules installed in parallel along with their characteristic dimensions.

2.3. Feed solution

A feed solution with high fouling tendency was prepared to expedite the biofouling development on UF membrane (total organic carbon - TOC = 323 mg/L, bacterial cell count = $4.61e^{+06}$ cells/mL from flow cytometer analysis). This solution composed of 4 g of Bacto™ Yeast Extract (Extract of Autolysed yeast cells, Becton Dickinson and Company) dissolved in 1 L of Red Sea water (Alpatova et al., 2018) and incubated for 24 h at 30°C. The prepared solution was then diluted with 3 L of Red Sea water. Throughout the filtration test, the final total volume

of feed was regularly adjusted up to 4 L with a freshly prepared solution having 1 g/L of Yeast Extract concentration.

2.4. Flow operating parameters and numerical approach

UF experiments were realized for all spacers with two different operating conditions: (i) constant inlet feed flow velocity (U_0 = 0.185 m/s) and (ii) variable U_0 conditions in order to trip opposite hydrodynamics from steady to unsteady state or vice-versa. In the latter case, the inlet feed flow velocities were chosen such that the hydrodynamics state is opposite as seen for the first case with constant U_0 (from steady to unsteady state or vice versa). These employed operating parameters are summarized in Table 1. The fluid behaviors inside the filtration channel of all tested spacers were computationally investigated by using DNS (Qamar et al., 2019). A same numerical methodology already described elsewhere (Kerdi et al., 2018) was followed in this study.

Table 1. Operating parameters utilized during the filtration processes with various tested pillar feed spacers. D_F, Ɛ, U_0 and Q represent the filament diameter, porosity of filtration channel, inlet feed flow velocity and volumetric feed flow rate, respectively. Clearance (h) represents the physical distance from the filament outer surface to the membrane surface.

Experimental cases	Feed spacer	D_F (µm)	h (µm)	Ɛ	U_0 (m/s)	Q (mL/min)
Constant U_0	P-340	340	430	0.922	0.185	200
	P-500	500	350	0.889	0.185	200
	P-1000	1000	100	0.704	0.185	200
Varied U_0	P-340	340	430	0.922	0.496	550
	P-500	500	350	0.889	0.389	432
	P-1000	1000	100	0.704	0.092	100

3. Results and discussion

To explicitly quantify the hydrodynamics and the geometric role of feed spacer on membrane biofouling, two sets of experiments under varying hydrodynamics conditions (Section 2.4 - Table 1) are performed using different pillar spacers having filament diameters of 340 µm, 500 µm and 1000 µm (different clearance region heights). Prior to filtration experiments, pressure drop measurements inside the filtration channel were performed to evaluate the intrinsic ability of each spacer to minimize the required energy and to validate the DNS simulations. Subsequently, results of filtration experiments in terms of permeate flux production are presented. Finally, the hydrodynamics and spacer geometric correlation with biofouling adhesion and growth are thoroughly investigated.

3.1. Channel pressure drop to anticipate energy requirements for various pillar spacers

Channel pressure drop is a suggestive parameter of relative energy consumption by different types of feed spacers. A higher channel pressure drop would account for higher energy consumption if all other filtration parameters are kept the same (inlet velocity, transmembrane pressure and channel thickness) (Karabelas et al., 2018). Therefore, to gauge the energy efficiency of the pillar spacers in absence of fouling phenomena, initial pressure drop gradients of filtration channels are experimentally evaluated. Figure 2a presents the variation of initial channel pressure drop gradients ($\Delta P/\Delta L$, ΔP is the differential value of pressures measured inside the channel through pressure probes placed at a distance L as depicted in Figure 1) as a function of inlet feed flow velocity (U_0) in a range of 0.046 - 0.507 m/s. For commercial spacer, the typical pressure drop for 34 Mil (~ 0.863 mm) thick spacer having feed velocity in the range of 0.01 - 0.2 m/s is generally between 10 - 450 mbar/m (Haaksman et al., 2017; Vrouwenvelder et al., 2009b).

The feed channel pressure drop is determined by e.g. the spacer geometry, thickness, porosity and cross flow velocity.

In agreement with other studies (Ahmad and Lau, 2006; Ali et al., 2019), pressure drop gradients tend to increase with the rise of velocity regardless of the spacer type. As seen in Figure 2a, P-1000 spacer had the highest pressure drop gradients at all U_0 followed by P-500 and P-340 spacers. This descendant order of pressure drop gradient curves for the various spacers was in correlation with their correspondent channel porosity (Ɛ) values, where P-1000 spacer constitutes least channel porosity (Ɛ = 0.704) followed by P-500 (Ɛ = 0.889) and P-340 (Ɛ = 0.922) (Table 1). At inlet velocity of U_0 = 0.185 m/s, the experimental values of pressure drop gradients were estimated to be 55 mbar/m and 141 mbar/m inside the filtration channels of P-340 and P-500, respectively. However, these values increased roughly 8 to 3 times respectively in presence of P-1000 spacer where $\Delta P/\Delta L$ reached 432 mbar/m at the same velocity. In accordance with previous studies (Ali et al., 2019; Schwinge et al., 2002b), it can be inferred that as the height of clearance region decreases (spacer filament diameter increases), the pressure drop gradient of the correspondent spacer increases for a fixed channel height. Contrary to the thickest spacer (P-1000), a negligible loss in pressure was observed with the spacer having the thinnest filament diameter (P-340) at low extent of inlet velocities (U_0 < 0.092 m/s). It is noteworthy to highlight here that even though the used channel height (H = 1200 µm) in UF do not mimic typical RO channel height process (H < 900 µm), the trend of initial pressure drop gradients for various tested spacers (having various filament diameters) is predicted to be maintained in RO process as it is mainly related to the channel porosity, spacer design and feed flow rate for each spacer. On the other side, the range of applied U_0 magnitudes to measure the initial pressure drop gradient variation covers the magnitudes commonly operated in RO (U_0 = 0.16 - 0.20 m/s). Therefore,

this study is mainly pertinent to the UF process but its insights might allow a basic understanding for anticipating the biofilm/hydrodynamics map and the initial energy consumption plausibly occurred in NF and RO processes, since they all have similar spiral wound membrane module configuration with similar spacer geometries and therefore similar hydraulics and pressure drops.

Furthermore, computational pressure drop gradients are also determined by DNS calculations for the two operating cases and are presented in Figure 2b. These calculated pressure drop gradients exhibited consistent values with those experimentally measured, thereby establishing the validity of the model.

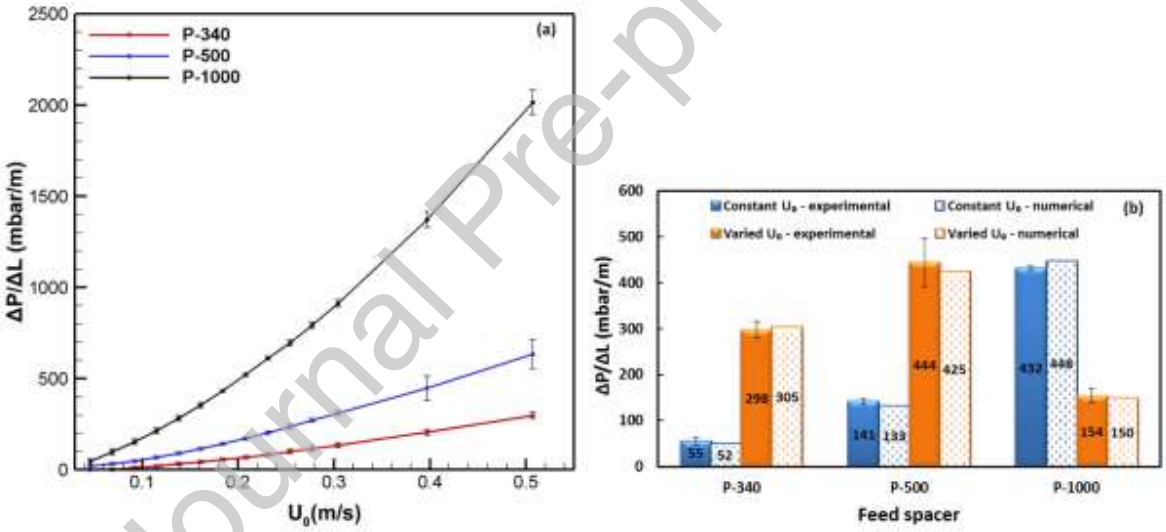

Fig. 2. Experimental differential pressure drop gradient variation as a function of inlet feed flow velocity U_0 (a), and comparison of numerical/experimental differential pressure drop gradients for both operating cases: constant inlet velocity (U_0 = 0.185 m/s) and varied inlet velocities applied (U_0 = 0.496 m/s for P-340, U_0 = 0.389 m/s for P-500, and U_0 = 0.092 m/s for P-1000) (b), in presence of various tested pillar spacers.

3.2. Permeate flux production to evaluate filtration performance for various pillar spacers

The impact of varying the filament diameter of pillar spacers (clearance region) on permeate flux production was evaluated at two different operating conditions as presented in Table 1. Permeate fluxes were then recorded over time throughout UF experiments and plotted in Figure 3 for different tested spacers.

Regardless of the operating conditions and the spacer configuration, permeate flux profiles followed the same trend of decrease during the filtration process. A sharp decline was observed in the first sixteen hours until steady flux values are reached (Fig. 3a,b). At constant inlet velocity (U_0 = 0.185 m/s) (Fig. 3a,c), highest amount of flux passing through the membrane equipped by P-1000 spacer was recorded with an average value at steady state (J_{av}) estimated to be 16.5 LMH. Simultaneously, half of this amount (J_{av} = 8.6 LMH) was obtained by reducing in half the filament diameter (P-500). However, the spacer with thinnest filament diameter (P-340) produced the lowest average flux quantity (J_{av} = 4.7 LMH) at the same inlet velocity. These findings demonstrated that the amount of produced permeate flux improved significantly when a decrease of clearance region between the filament spacer and UF membrane (rise of filament diameter) was achieved for the same applied inlet feed velocity.

Compared to the first operating case, an opposite behavior was observed in case of varied U_0 applied (Fig. 3b,c). At this operating condition, the lowest average steady flux was achieved by P-1000 spacer (J_{av} = 14.8 LMH) where a lower inlet feed velocity was used (U_0 = 0.092 m/s, Table 1). On the other hand, higher average permeate fluxes were collected in presence of thinner spacers P-340 (J_{av} = 23.0 LMH) and P-500 (J_{av} = 20.2 LMH) at applied cross-flow velocities of U_0 = 0.496 m/s and 0.389 m/s, respectively.

Based on pressure measurement and flux performance, it is challenging to identify which spacer filament diameter (or clearance height) is ideal for UF process if the filtration channel height is fixed. Thus, specific flux (J_{sp}) which represents flux produced per unit of pressure drop (LMH/mbar) is an ideal parameter to gauge the performance of the various spacers. Figure 3d shows the average specific flux values obtained for various spacers under different flow conditions. It is clear that P-1000 spacer at lower cross-flow velocity (U_0 = 0.092 m/s) has the highest specific flux (J_{sp} = 1.9 LMH/mbar), followed by P-340 spacer (J_{sp} = 1.7 LMH/mbar) at U_0 = 0.185 m/s. Hence, in terms of filtration performance, P-1000 is ideal at lower inlet velocities. However, in terms of energy requirement, this spacer might not be a potential candidate for long term filtration as biofouling rate for thick spacer is higher as demonstrated in the subsequent sections.

Journal Pre-proof

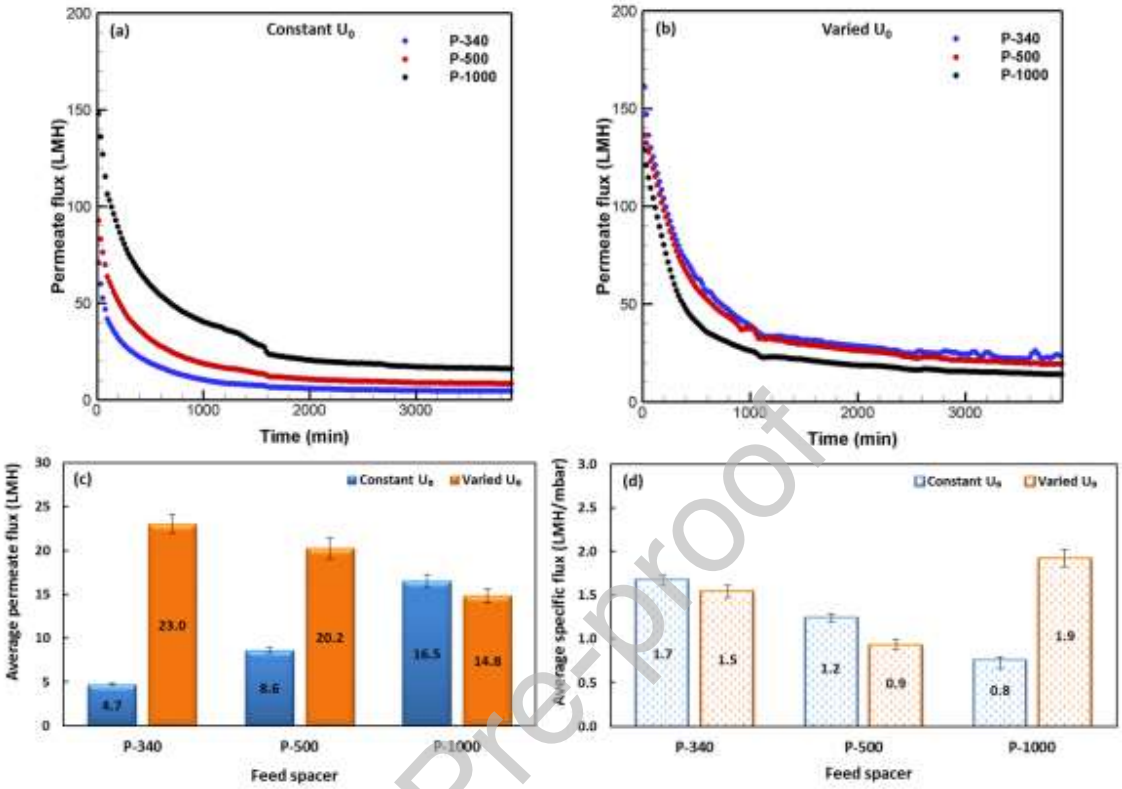

Fig. 3. Evolution of permeate flux over the evolvement of filtration process in presence of various tested pillar spacers at two different operating parameters: constant inlet feed flow velocity (U_0 = 0.185 m/s) (a) and varied U_0 (U_0 = 0.496, 0.389 and 0.092 m/s for P-340, P-500 and P-1000, respectively) (b) along with average permeate fluxes produced (c) and average specific permeate fluxes (d) determined at steady state conditions for various pillar spacers.

3.3. Biofouling development under various hydrodynamics conditions inside the filtration channel

Optimization of feed spacers inside the filtration channel has been considered in previous research studies in terms of spacer dimensions (Koutsou et al., 2007; Siddiqui et al., 2016), orientation (Neal et al., 2003), design and thickness (Kerdi et al., 2018; Koutsou and Karabelas, 2015) aiming to enhance permeate flux production while minimizing pressure drop, thereby lowering

energy consumption. In biological active feed, the flux production and the rise in pressure drop are directly related to the biofouling developed inside the spacer filled channel (Sreedhar et al., 2018; Vrouwenvelder et al., 2009a). As biofouling is influenced by hydrodynamics conditions (Purevdorj et al., 2002; Shen et al., 2015), it is crucial to deeply understand the role of hydrodynamics shear stress on biofouling adhesion and propagation, especially on membrane surface. Although accurate predictions on hydrodynamics and the associated shear stress can be achieved by highly resolved space and time DNS simulations (Qamar et al., 2019), it is still challenging to gauge experimentally hydrodynamics in a filtration channel. In the current study, DNS simulations (validated by using pressure drop data presented in Section 3.1) are carried out by using exact computer aid-design (CAD) of the tested pillar spacers. All simulations are performed in time dependent mode and the flow inside the channel is either settled to steady or unsteady state depending on spacer type and inlet feed flow conditions. Simulated results are further correlated to the biofouling development which is monitored by OCT scans.

3.3.1. Correlating hydrodynamics and biofouling development at constant inlet feed velocity

3.3.1.1. Effect on localized velocity distributions for different spacers at constant inlet feed velocity

The variation in spacer filament diameter results in varying the clearance region between the spacer filament and the membrane surface. This fundamental change will influence the incoming feed flow, thereby alternating the local hydrodynamics for each spacer case.

Figure 4 shows the local velocity distributions obtained through DNS simulations in a plane near the membrane surface (z = 60 µm) for the three tested spacers at constant U_0 = 0.185 m/s. It can be inferred immediately that the hydrodynamics is steady in nature for thin spacers P-340 and P-500 (Fig. 4a,b), while it quickly transits to unsteady state for thick spacer P-1000, as depicted by

Journal Pre-proof

spatial fluctuations (Fig. 4c). Further, the local velocities inside the spacer unit cells as well as under the filaments increase with the increase of spacer filament diameter. This is attributed to the clearance region created between the filament and the membrane surface. The height of this clearance region (calculated to be 430, 350 and 100 µm on each side of the spacer filament for P-340, P-500 and P-1000 spacers, respectively, as shown in Table 1) tends to decrease as the filament diameter increases resulting in increasing the local velocity, especially under the filaments. As the inlet velocity is fixed (flow rate fixed), the same volume of feed flow had to pass under the filaments which act as obstructions towards the flow in the filtration channel. As a result, local velocity under the spacer filaments has to increase (with highest magnitude for lowest clearance) in order to maintain the mass conservation resulting in altering significantly the local velocity (Gimmelshtein and Semiat, 2005). Subsequently, the highest velocities (represented by green and red colors in Fig. 4a,b and Fig. 4c, respectively) are observed under the filaments and are estimated approximately in the range of 0.14 - 0.2 m/s, 0.18 - 0.26 m/s and 0.9 -1.05 m/s under the filaments for the P-340, P-500 and P-1000 spacers, respectively.

On the other side, the vertical pillars (filament intersection nodes) which act as obstructions to the incoming fluid stream force the feed flow to bifurcate resulting in a lower velocity magnitude (represented by blue color) behind the pillars. This low magnitude of local velocity is found to sweep the majority area of the membrane inside the spacer cell. At the back face of the pillars, separated vortices remain attached in the case of steady flow resulting in dead zones (flow recirculating regions for nutrient/particulate accumulation), as shown schematically in the case of P-340 and P-500 spacers (Fig. 4a,b). These dead zones are known to be optimum regions prone to the accumulation of foulant particles (Ali et al., 2019). However, the attached vortices were found quickly destabilized in the case of P-1000 because of unsteadiness (Qamar et al.,

2012) resulting in eliminating the attached dead zones (vortices breakdown schematically shown in Fig. 4c).

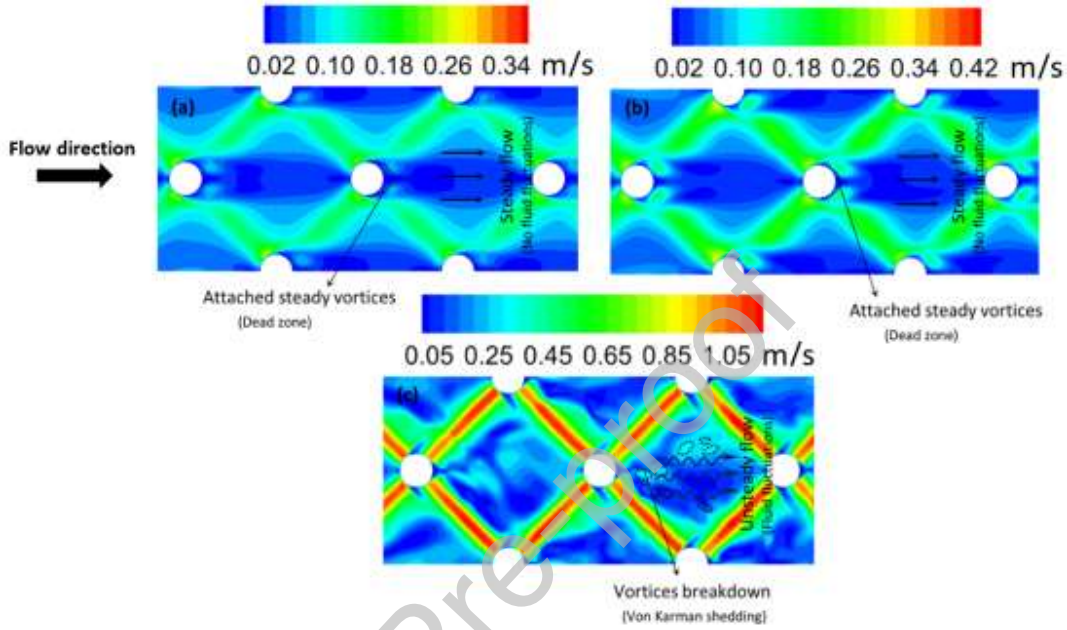

Fig. 4. Velocity contours at plane near the membrane wall for different pillar spacers: P-340 (a), P-500 (b) and P-1000 (c) at constant inlet velocity (U_0 = 0.185 m/s). The arrows represent the flow direction and the hydrodynamics state in filtration channels.

3.3.1.2. Influence on fluid shear stress at constant inlet feed velocity for different spacers

Local fluid shear stress distribution, originating due to change in spacer design, is critical to know in advance to correlate the biofilm growth behavior. Spatial shear stress distributions were further calculated on the spacer and membrane surfaces at constant U_0 = 0.185 m/s, and depicted in Figure 5. As the spacer filaments and the supporting pillars are the major components obstructing the incoming fluid flow, it is expected that the front face of these filaments should experience the highest shear force. Figures 5a,b clearly show this flow pattern for thin spacer filaments (P-340 and P-500). It is noteworthy here that for thin filaments (steady cases), the

whole front face area has high shear stress (Fig. 5a,b). Whereas, for thicker filament P-1000, the shear stress has highest values on the top and bottom of the filaments (Fig. 5c). From fluid mechanics perspective, this phenomenon is associated to blocking effect (Tritton, 2012). Spacer with thicker filaments (P-1000) and low clearance region (100 µm) tends to stagnate more fluid ahead of the filaments as compared to spacers with thin filaments and larger clearances (430 and 350 µm for P-340 and P-500, respectively). As a result, high shear stress locations on filament surfaces are different in case of thin and thick filament spacers as schematically represented in the insets of Figure 5 (cross-sectional views of spacer filaments). Furthermore, as the overall hydrodynamics is unsteady in nature for the thick filament spacer, fluctuating shear stress values ($\sim$ 1 - 24 N/m^2) are also observed in front and back faces of the thick filaments (Fig. 5c).

On the membrane surface, the highest shear stress magnitude zones are predictably located under the filaments resulted from the creation of narrow spaces which led to intensify the local velocity at these regions (Koutsou et al., 2018) as previously observed in local velocity distributions (Fig. 4). The magnitude of fluid shear stress induced under the filaments of P-340 and P-500 spacers was estimated to be in close range ($\sim$ 3 - 7 N/m^2) (Fig. 5a,b). However, the shear stress magnitude under the filaments of P-1000 spacer was found to be significantly higher (almost eight times, $\sim$ 34 - 40 N/m^2) (Fig. 5c). Although these high shear stress regions help to improve the mass transfer (Schwinge et al., 2002a), it might be considered as the favorable locations for the seeding/attachment of bacteria followed by their spreading over the membrane surface (Lecuyer et al., 2011; Radu et al., 2010; Saur et al., 2017). Thus, to explore this hypothesis, the attachment and growth of biofouling on spacer filament and membrane surface are monitored during UF operation with time by using OCT characterization.

Journal Pre-proof

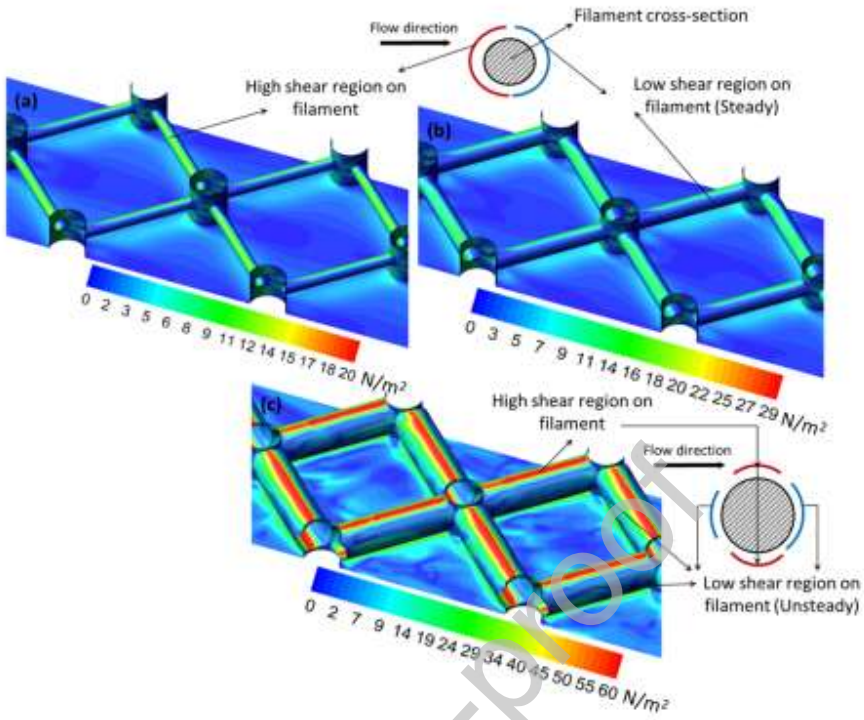

Fig. 5. Shear stress contours at plane near the membrane wall for different pillar spacers: P-340 (a), P-500 (b) and P-1000 (c) at constant inlet velocity (U_0 = 0.185 m/s). Schematics of cross-sectional spacer filaments described the shear hydrodynamics are illustrated in the insets.

3.3.1.3. Mapping biofilm attachment/growth for different spacers at constant inlet velocity

The biofouling attachment and growth appear to be considerably influenced by the shear stress distribution and the clearance space between the spacer filaments and the membrane surface. *In-situ* OCT images were thus taken on filament spacers (Fig. 6(I-III)b) and membrane surface; (i) at region close to the filament having high shear stress (along line L_3 in Fig. 6(I-III)g) and (ii) at central region of spacer cell where lower shear stress is predicted by simulations (along line L_2 in Fig. 6(I-III)g).

Journal Pre-proof

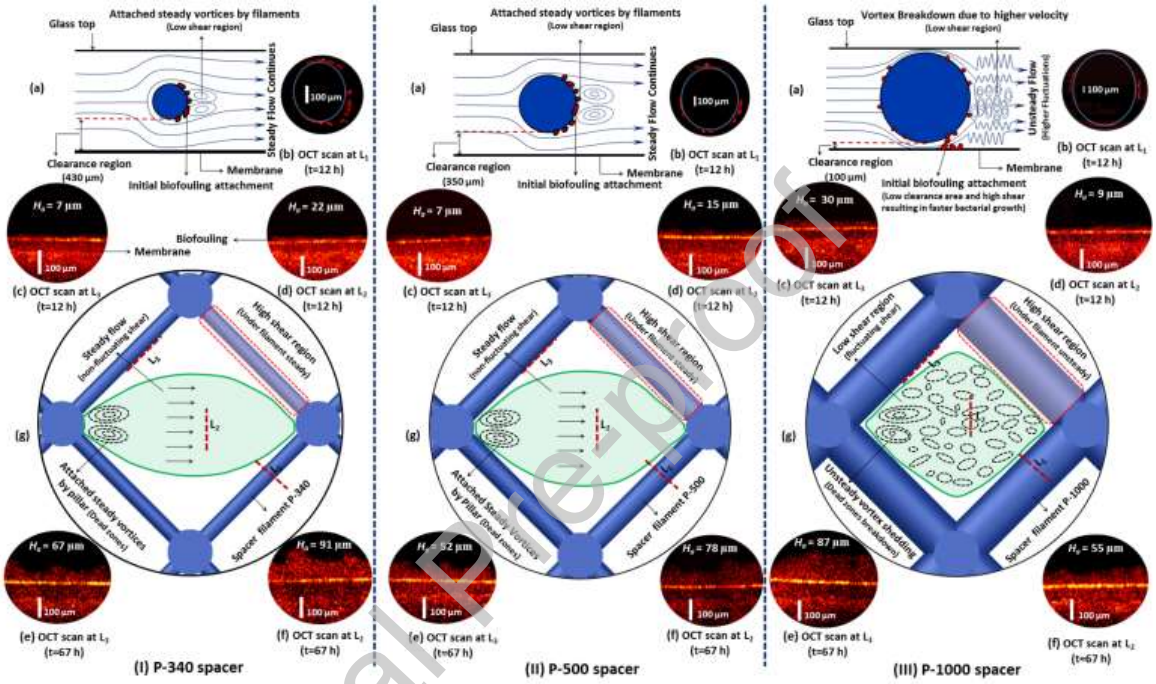

Fig. 6. Mapping the biofilm attachment/growth with hydrodynamics conditions at constant inlet feed velocity and OCT images for various pillar spacers: (I) P-340, (II) P-500 and (III) P-1000. For each spacer, (a) represents the cross-sectional schematics of hydrodynamics/biofouling around the spacer filament; (b) is OCT scan taken on the filament at line L_1; (c) and (d) are OCT scans taken on membrane surface after 12 h of biofouling development at lines L_3 and L_2, respectively; (e) and (f) represent OCT scans taken on membrane surface after 67 h of biofouling development at lines L_3 and L_2, respectively; and (g) is the schematics illustrated the hydrodynamics inside the whole unit spacer cell. H_a is the average of maximal and minimal biofilm thicknesses visualized in each OCT image.

Journal Pre-proof

At early stage of biofilm formation (12 h), bacterial attachment signs are observed on the spacer filament. For thin pillar spacers (P-340 and P-500), the biofilm adhesion looks roughly similar along the circumference of spacer filaments and appears to be higher than P-1000 filament spacer (Fig. 6(I-III)b). This lower biofilm attachment observed in case of P-1000 is potentially a result of unsteady hydrodynamics conditions (flow fluctuations) obtained on front and back faces of P-1000 filaments compared to steady hydrodynamics conditions encountered by thin spacers (Fig. 6(I-III)a, Fig. 5). Furthermore, the initial biofilm attachment on thin spacer filaments (P-340 and P-500) is found higher on back face of the filaments where it experiences a lowest shear stress environment on the filament (solid surface) (Fig. 5a,b). However, for P-1000 case, the initial bacteria attachment can be found more pronounced in front and back faces where shear stress is low as explained in above Section 3.3.1.2 (Fig. 5c). More bacteria attachment is expected in the low shear region, especially for steady hydrodynamics cases (P-340 and P-500), where attached vortices also aid in entrapping nutrients as depicted schematically in Fig. 6(I-II)a.

Contrary, on the membrane surface (porous material), the area close to the filaments appears much cleaner for thin spacers (H_a ~ 7 µm thick biofilm) than for thick spacer P-1000 where a biofilm layer of H_a ~ 30 µm was observed after 12 h of filtration process (Fig. 6(I-III)c). Under the same inlet flow velocity, the shear stress distribution demonstrated that the highest magnitude on membrane surface was observed under the filaments of P-1000 spacer (Fig. 5). Besides the presence of high shear, this thickest filament spacer (P-1000) has the lowest clearance region which led to stagnating more fluid, thereby promoting faster growth of bacteria under filaments. The present low clearance region facilitates then the migration of bacteria from spacer filament to membrane surface as schematically depicted in Figure 6(III)a. However, OCT images that were taken at central region of the membrane revealed lower biofouling growth for P-1000 (H_a ~

9 µm) after 12 h of filtration compared to the other spacers (H_a ~ 22 µm and 15 µm for P-340 and P-500, respectively) (Fig. 6(I-III)d). This is attributed to the prevalence of unsteady flow environment inside P-1000 spacer cells. Therefore, it is clear that initial attachment/seeding on membrane (porous material) primarily dependent on hydrodynamics conditions, and faster attachment happens in the region of high shear and low clearance.

When filtration progressed to its steady state condition (67 h), OCT scans for thin spacers (P-340 and P-500) demonstrated that the biofouling developed in the area near the filament was less than this developed in the central spacer cell location (Fig. 6(I-II)e,f). Contrariwise, thick spacer cells (P-1000) were found to have the least biofilm thickness in the central region (H_a ~ 55 µm) (Fig. 6(III)e,f). Simultaneously, the shear stress distributions exhibited that the region on membrane surface near the filaments had the highest shear stress while the central spacer cell region had the lowest for all spacers (Fig. 5). It appears that the bacterial adhesion is initially faster under the filaments (Ali et al., 2019; Kerdi et al., 2020; Kerdi et al., 2018) and later biofilm propagates and grows faster towards the lower shear region (center of cell spacer). This hypothesis is confirmed in case of thin spacers (P-340 and P-500) where lower fluid shear stress is detected in the central region and the flow is steady in nature leading to rising the biofilm growth potential (Fig. 6(I-II)f,g). However, the flow unsteadiness which is generated in case of thick spacer (P-1000) hampers the growth of biofilm in the central area of spacer cells resulting in lowest biofilm thickness, as shown in Figure 6(III)f,g.

Similarly to our observations on membrane surface, high shear stress/velocity regions underpinned with stagnant nutrient locations were found to drastically trigger the initial bacterial attachment on the surface (Aufrecht et al., 2019; Persat et al., 2014). Subsequently, during the initial phase of biofilm formation, the presence of a high hydrodynamic shear environment

promotes, in turn, production of EPS resulting in strong initial bacterial cell adhesion on the substratum (Liu and Tay, 2002). The amount of produced EPS and the bacterial growth mechanism vary as a function of the surface characteristics (Becker, 1996). It has been demonstrated that bacteria once seeded on the material surface in a porous network, tend to grow continuously in the flow downstream direction with a bacterial movement directed across the velocity gradients (Aufrecht et al., 2019). The development and impact of biofilm streamers in spacer filled channels have been reported (Creber et al., 2010), confirming the results of our study.

Based on the aforementioned findings, the biofouling pattern was found to be very well correlated with the shear stress map at constant feed velocity inlet. As it has been reported that the attachment of bacteria on the substratum is substantially influenced by its intrinsic characteristics such as porosity, roughness, rigidity, topography, material type, etc. (Charman et al., 2009; Elftonson et al., 1996; Siddiqui et al., 2019), it was crucial to monitor the response of bacterial attachment taken place on both spacer and membrane surfaces (having different properties) towards the variation of hydrodynamics conditions. On spacer surface (which is a non-filtrating surface), biofouling prefers to first attach itself at lower shear region. Whereas, on membrane surface (filtration surface), initial biofouling adhesion region is close to the spacer filament where shear stress magnitudes are higher. Further, propagation and spread of the biofilm depends on the clearance region and the access to the low hydrodynamics shear regions. The bacteria deployed on membrane surface (with high attachment potential for low clearance region) would prefer to grow faster in the region of low shear and steady flow conditions than in the high shear and unsteadiness environment as observed in the present cases.

Journal Pre-proof

Journal Pre-proof

3.3.2. Correlating hydrodynamics and biofouling development at varied inlet velocity

This set of experiments was achieved in order to confirm the dependence of biofouling growth pattern on shear stress hydrodynamics and clearance region height. In this operating case, the inlet flow velocities were significantly altered to reverse the hydrodynamics situations as seen in the above case (Sections 3.3.1). For P-340 and P-500, the feed inlet velocities were increased until the hydrodynamics state switches from steady to unsteady (U_0 = 0.496 and 0.389 m/s for P-340 and P-500, respectively). While, for P-1000 spacer, the applied inlet velocity was significantly reduced (U_0 = 0.092 m/s) in order to trip the flow to steady state inside the feed channel (Table 1).

3.3.2.1. Effect on localized velocity distributions for different spacers at varied inlet velocity

DNS calculations clearly revealed that under these conditions unsteady state is successfully achieved for P-340 and P-500 where more perturbed local velocity magnitudes were visualized in the central area of the spacer cells (Fig. 7a,b). As a result, lower and higher velocity magnitude fluctuations (~ 0.02 - 0.26 m/s) were then detected in this area. Conversely, a steady state was established with P-1000 spacer confirmed by the lack of fluctuations, and low magnitude of local velocity (~ 0.02 m/s) was found to predominate the entire central area of spacer cells (Fig. 7c).

Journal Pre-proof

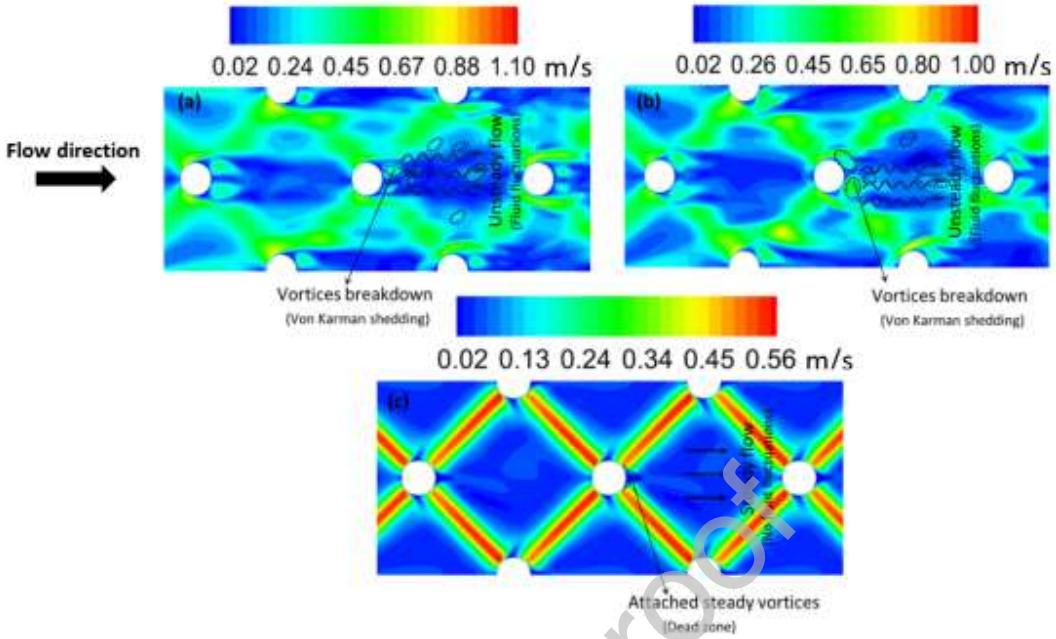

Fig. 7. Velocity contours at plane near the membrane wall for different pillar spacers: P-340 (a), P-500 (b) and P-1000 (c) at varied inlet velocity. The arrows represent the flow direction and the hydrodynamics state in filtration channels.

3.3.2.2. Influence on fluid shear stress at varied inlet feed velocity for different spacers

The highest shear stress is still found on the filaments of all spacers. However, as the flow is completely tripped for each case (steady to unsteady and vice-versa), the thinner spacer filaments show fluctuating shear stress on the filaments contrary to thicker spacer filaments (Fig. 8). For this operating case, the maximum shear stress region on the membrane surface was observed under the filaments of spacers. The shear magnitudes were approximatively calculated in the range of ~ 9-14 N/m^2, 10 - 25 N/m^2 and 11 - 28 N/m^2 for P-340, P-500 and P-1000, respectively. Although for P-340 and P-500, the flow is tripped to unsteady state, the local shear stress is found to be lowest on back face of the pillars, as shown in Figures 8a,b. For this case, it is relevant to emphasize that as the filament size increases (the corresponding inlet velocity decreases (Table 1)), the low shear region (green region marked schematically in Fig. 9(I-III)g)

behind the pillars spreads out. As a result, the low shear area remains limited in the central region of thin spacers (P-340 and P-500) compared to thick spacer (P-1000) where low steady shear stress values were found fully covered in the entire central region of the membrane inside the spacer cell (Fig. 8c).

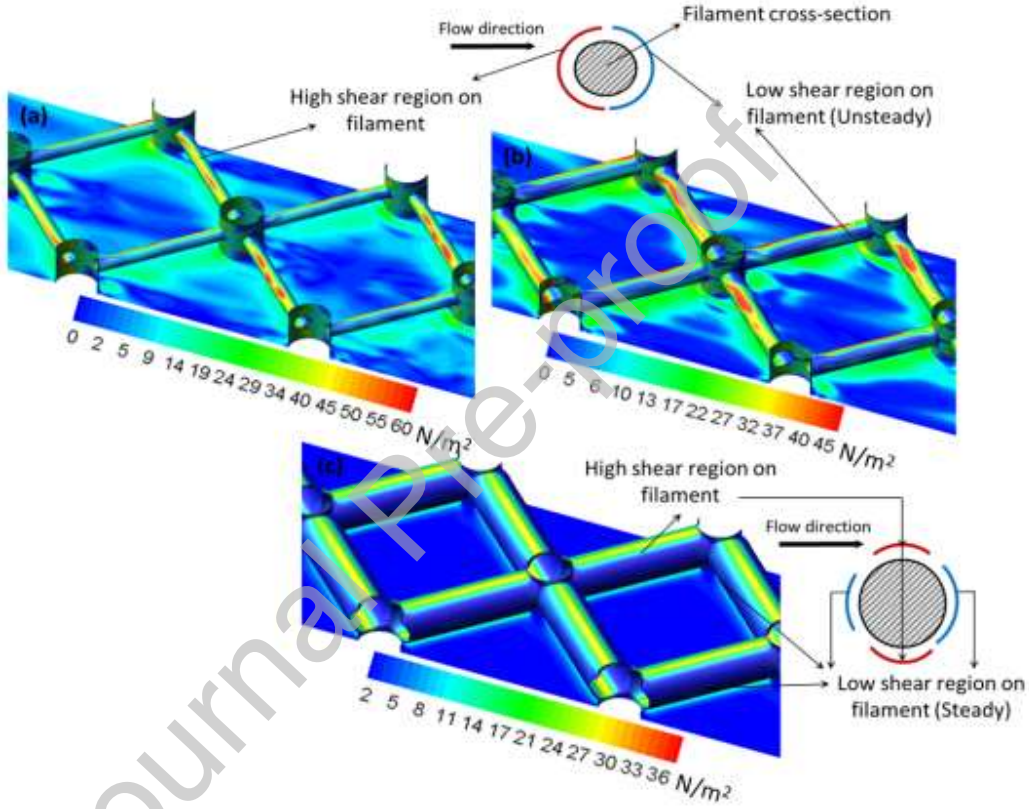

Fig. 8. Shear stress contours at plane near the membrane wall for different pillar spacers: P-340 (a), P-500 (b) and P-1000 (c) at varied inlet velocity. Schematics of cross-sectional spacer filaments described the shear hydrodynamics are illustrated in the insets.

3.3.2.3. Mapping biofilm attachment/growth for different spacers at varied feed inlet velocity

Based on the fluid shear stress distribution, similar biofouling growth pattern of constant inlet velocity case (Section 3.3.1.3) was also proved in these operating conditions where

hydrodynamics was completely reversed for all spacers. For early filtration stage (12 h), biofouling attachment is relatively lower on thin spacer filaments (P-340 and P-500) because of the presence of unsteady fluctuation shear stress compared to P-1000 spacer (steady non-fluctuating shear stress) (Fig. 9(I-III)a,b). Moreover, the biofouling is observed randomly placed on circular filaments (non-filtration surface) of thin spacers indicating the presence of hostile environment on their filament surfaces due to fluctuation in shear stress resulting in reducing the bacterial attachment (Fig. 9(I-II)a).

On membrane surface (filtration surface), the biofouling pattern appears to respond accordingly to the hydrodynamics shear stress distribution. At 12 h of filtration process, P-340 has slightly less biofouling (H_a ~ 13 µm) than P-500 (H_a ~ 16 µm) as shear stress calculated under its filaments is slightly lower (Fig. 9(I-II)c). However, OCT image revealed that more biofouling (H_a ~ 74 µm) was visualized under the filaments of P-1000 where relatively high shear stress associated with lowest clearance was identified (Fig. 9(III)c). Furthermore, the central region for all spacers has higher biofilm growth compared to near the filament area at 67 h of filtration (Fig. 9(I-III)e,f). Central region of P-1000 which has the lowest shear and steady hydrodynamics is found to have the highest biofouling cake (H_a ~ 196 µm) (Fig. 9(III)f). For P-340 and P-500 spacers (Fig. 9(I-II)f), the biofouling is less at central spacer cell location compared to P-1000 spacer (H_a ~ 102 µm and 133 µm for P-340 and P-500, respectively) as for these spacers the inlet conditions result in unsteady flow conditions inside the filtration channels (Fig. 9(I-III)g). Further, digital snapshots of the biofouling on the membrane surface are also presented for 67 h. As previously predicted by DNS simulations (Fig. 8), the low shear region has clearly the highest biofouling. Moreover, this low shear region spreads out (due to reduction

in incoming velocity) as the filament diameter increases. These digital photography show that the biofouling maps appropriately the low shear region for each spacer.

Journal Pre-proof

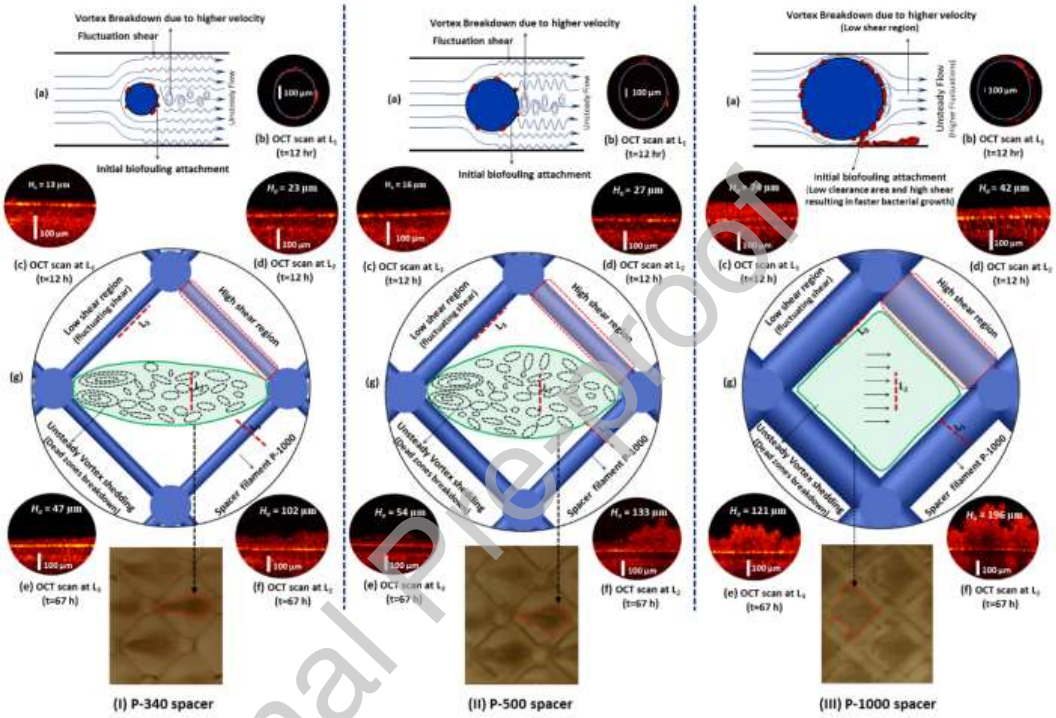

Fig. 9. Mapping the biofilm attachment/growth with hydrodynamics conditions at varied inlet feed velocity and OCT images for various pillar spacers: (I) P-340, (II) P-500 and (III) P-1000. For each spacer, (a) represents the cross-sectional schematics of hydrodynamics/biofouling around the spacer filament; (b) is OCT scan taken on the filament at line L_1; (c) and (d) are OCT scans taken on membrane surface after 12 h of biofouling development at lines L_3 and L_2, respectively; (e) and (f) represent OCT scans taken on membrane surface after 67 h of biofouling development at lines L_3 and L_2, respectively; and (g) is the schematics illustrated the hydrodynamics inside the whole unit spacer cell. Digital photography taken on the top of filtration channel showing the biofouling grown on membrane surface well correlated with the low shear region of the spacer cell. H_a is the average of maximal and minimal biofilm thicknesses visualized in each OCT image.

Journal Pre-proof

Journal Pre-proof

4. Perspective and outcomes

Based on the above experimental and numerical findings, it is clear that hydrodynamics play a significant role on biofilm evolution and growth. Inside the filtration channel, the biofilms on spacer (impermeable surface) and membrane (permeable surface) have different affinity. On spacer surface, the biofilm prefers to grow in the region of low shear where hydrodynamics fluctuations are minimal. Thus, if the overall hydrodynamics inside the filtration channel is steady, the growth of biofilm on the spacer surface is more favorable (Fig. 6(I-II)b). Propagation of biofilm from the spacer to the membrane surface is more assertive if the clearance region is small (Fig. 6(III)a and Fig. 9(III)a).

Similarly, locally on the membrane surface, during early stages of filtration (12 h), the region under the filaments (high shear region) tends to have higher biofouling. As its corresponding occupied area is low relative to the entire active area (Fig. 5 and Fig. 8), it should not significantly influence the filtration performance if the remaining membrane area is relatively clean (like for thin filament spacers, P-340 and P-500). The initial biofouling under the filaments is aggravated by two possibilities: (i) if it is the region closest to the spacer surface, and (ii) the feed velocity component normal to the membrane is high resulting in greatly depositing nutrient and organic materials under the filaments. Thus, during initial hours of filtration, biofilm growth is visible more under the filaments compared to the central region of the spacer cell as seen in case of P-1000 spacer (Fig. 6(III)c,d and Fig. 9(III)c,d). As time progresses, the low shear region is more favorable to the proliferation of bacteria. They thrive effectively and outrun the growth under the filaments (Fig. 6(I-II)e,f and Fig. 9(I-III)e,f). Further, the presence of unsteadiness effectively helps in mitigating the biofilm growth as seen from two operating conditions (Fig. 6(III)e,f and Fig. 9(I-II)e,f).

From application perspective, it is clearly evident from specific flux data that thick filament spacer appears to perform best and produces highest flux per unit pressure drop (J_{sp} ~ 1.9 LMH/mbar - Fig. 3d). However, the biofilm growth for thick filament spacer is highest at low U_0 (case of Fig. 9(III)f). For long term operation, the local channel pressure drop due to the biofilm growth (reduced channel porosity) would be significantly higher and would ultimately tarnish the energy requirement of the filtration process. Thus, thick filament spacer (P-1000) should not be a choice for long term filtration or in cases of high risk of biofouling. On the other side, the thin spacer (P-340) seems quite favorable in this scenario. The specific flux is relatively close to the thick filament spacer (J_{sp} ~ 1.7 LMH/mbar) and the biofilm growth inside the filtration channel appears to be least (Fig. 6(I)f). Therefore, in long term operation, the use of thin filament spacer helps to consume less energy (due to its least pressure drop) and would perform best much without negatively effecting the overall filtration performance.

Compared to the P-1000 thick filament spacer, the thinner filament P-340 spacer has an initial lower pressure drop, but with time there is more biofilm development and a related higher pressure drop. The P-340 spacer has more open space (higher porosity) possible enabling a better removal of detached and solubilized biofilm from the spacer and membrane out of the module, restoring the original low pressure drop. When a biofilm cleaning is efficient to restore the original performance then this spacer would be preferred for practice. Further studies are needed to evaluate the biofilm cleaning efficiency of the thick and thin filament feed spacers. Promising could be chemical (Sanawar et al., 2019), hydraulic (Radu et al., 2012) and gas bubbles (Alpatova et al., 2020) cleaning strategies.

Journal Pre-proof

Journal Pre-proof

5. Conclusions

The mapping of "shear stress hydrodynamics/clearance region" and "biofouling development" inside the filtration channels was clearly identified in this study. Three pillar spacers of the same pillar orientation, diameter and height, differing in filament diameters (340, 500 and 1000 µm) were employed to explore the biofouling response against varying the hydrodynamics states and clearances. Essential outcomes could be concluded as:

- At constant inlet cross-flow velocity, the increase of filament diameter at fixed height filtration channel leads to increase the local velocity and generate more flow unsteadiness in central spacer cells resulting in enhancing the permeate flux.

- Regardless of spacer filament diameter, the highest shear stress magnitude appears on membrane surface under the spacer filaments. This magnitude tends to increase in this location as the spacer filament diameter increases. However, lower shear stress magnitude is consistently observed in the central region of spacer cells.

- Irrespective of flow conditions (steady or unsteady) inside the feed channel, biofilm adhesion on spacer surface is more predominant in the region having low shear stress (back face of the spacer filaments).

- On membrane surface, biofouling is mainly attached in the region close to the spacer filaments where high shear stresses are prevalent, associated along with low clearance height (case of P-1000). Once seeded on membrane, the presence of low shear stress/steady hydrodynamics in central regions of spacer enhances the fast growth of bacteria.

6. Acknowledgment

The research reported in this paper was supported by King Abdullah University of Science and Technology (KAUST), Saudi Arabia. The authors acknowledge help, assistance and support

from the Water Desalination and Reuse Center (WDRC) staff and KAUST Supercomputing Laboratory (KSL).

7. References

Ahmad, A.L. and Lau, K.K. 2006. Impact of different spacer filaments geometries on 2D unsteady hydrodynamics and concentration polarization in spiral wound membrane channel. Journal of Membrane Science 286(1), 77-92.

Ali, S.M., Qamar, A., Kerdi, S., Phuntsho, S., Vrouwenvelder, J.S., Ghaffour, N. and Shon, H.K. 2019. Energy efficient 3D printed column type feed spacer for membrane filtration. Water Research 164, 114961.

Alpatova, A., Alsaadi, A. and Ghaffour, N. 2018. Boron evaporation in thermally-driven seawater desalination: Effect of temperature and operating conditions. Journal of Hazardous Materials 351, 224-231.

Alpatova, A., Qamar, A., Al-Ghamdi, M., Lee, J. and Ghaffour, N. 2020. Effective membrane backwash with carbon dioxide under severe fouling and operation conditions. Journal of Membrane Science 611, 118290.

Araújo, P.A., Miller, D.J., Correia, P.B., van Loosdrecht, M.C.M., Kruithof, J.C., Freeman, B.D., Paul, D.R. and Vrouwenvelder, J.S. 2012. Impact of feed spacer and membrane modification by hydrophilic, bactericidal and biocidal coating on biofouling control. Desalination 295, 1-10.

Aufrecht, J.A., Fowlkes, J.D., Bible, A.N., Morrell-Falvey, J., Doktycz, M.J. and Retterer, S.T. 2019. Pore-scale hydrodynamics influence the spatial evolution of bacterial biofilms in a microfluidic porous network. PLOS ONE 14(6), e0218316.

Becker, K. 1996. Exopolysaccharide production and attachment strength of bacteria and diatoms on substrates with different surface tensions. Microbial Ecology 32(1), 23-33.

Bernstein, R., Belfer, S. and Freger, V. 2011. Bacterial attachment to RO membranes surface-modified by concentration-polarization-enhanced graft polymerization. Environmental Science & Technology 45(14), 5973-5980.

Charman, K.M., Fernandez, P., Loewy, Z. and Middleton, A.M. 2009. Attachment of Streptococcus oralis on acrylic substrates of varying roughness. Letters in Applied Microbiology 48(4), 472-477.

Creber, S.A., Pintelon, T.R.R., Graf von der Schulenburg, D.A.W., Vrouwenvelder, J.S., van Loosdrecht, M.C.M. and Johns, M.L. 2010. Magnetic resonance imaging and 3D simulation studies of biofilm accumulation and cleaning on reverse osmosis membranes. Food and Bioproducts Processing 88(4), 401-408.

Da Costa, A.R., Fane, A.G., Fell, C.J.D. and Franken, A.C.M. 1991. Optimal channel spacer design for ultrafiltration. Journal of Membrane Science 62(3), 275-291.

Elftonson, J.E., Ström, G., Holmberg, K. and Olsson, J. 1996. Adhesion of Streptococcus sanguis to porous and non-porous substrates with well-defined surface energies. Journal of Adhesion Science and Technology 10(8), 761-770.

Gimmelshtein, M. and Semiat, R. 2005. Investigation of flow next to membrane walls. Journal of Membrane Science 264(1), 137-150.

Haaksman, V.A., Siddiqui, A., Schellenberg, C., Kidwell, J., Vrouwenvelder, J.S. and Picioreanu, C. 2017. Characterization of feed channel spacer performance using geometries obtained by X-ray computed tomography. Journal of Membrane Science 522, 124-139.

Habimana, O., Semião, A.J.C. and Casey, E. 2014. The role of cell-surface interactions in bacterial initial adhesion and consequent biofilm formation on nanofiltration/reverse osmosis membranes. Journal of Membrane Science 454, 82-96.

Hijnen, W.A.M., Biraud, D., Cornelissen, E.R. and van der Kooij, D. 2009. Threshold concentration of easily assimilable organic carbon in feedwater for biofouling of spiral-wound membranes. Environmental Science & Technology 43(13), 4890-4895.

Huang, X., Guillen, G.R. and Hoek, E.M.V. 2010. A new high-pressure optical membrane module for direct observation of seawater RO membrane fouling and cleaning. Journal of Membrane Science 364(1), 149-156.

Kang, S. and Choi, H. 2005. Effect of surface hydrophobicity on the adhesion of S. cerevisiae onto modified surfaces by poly(styrene-ran-sulfonic acid) random copolymers. Colloids and Surfaces B: Biointerfaces 46(2), 70-77.

Karabelas, A.J., Koutsou, C.P., Kostoglou, M. and Sioutopoulos, D.C. 2018. Analysis of specific energy consumption in reverse osmosis desalination processes. Desalination 431, 15-21.

Kerdi, S., Qamar, A., Alpatova, A. and Ghaffour, N. 2019. An in-situ technique for the direct structural characterization of biofouling in membrane filtration. Journal of Membrane Science 583, 81-92.

Kerdi, S., Qamar, A., Alpatova, A., Vrouwenvelder, J.S. and Ghaffour, N. 2020. Membrane filtration performance enhancement and biofouling mitigation using symmetric spacers with helical filaments. Desalination 484, 114454.

Kerdi, S., Qamar, A., Vrouwenvelder, J.S. and Ghaffour, N. 2018. Fouling resilient perforated feed spacers for membrane filtration. Water Research 140, 211-219.

Koutsou, C.P. and Karabelas, A.J. 2015. A novel retentate spacer geometry for improved spiral wound membrane (SWM) module performance. Journal of Membrane Science 488, 129-142.

Koutsou, C.P., Karabelas, A.J. and Kostoglou, M. 2018. Fluid dynamics and mass transfer in spacer-filled membrane channels: Effect of uniform channel-gap reduction due to fouling. Fluids 3(1), 12.

Koutsou, C.P., Yiantsios, S.G. and Karabelas, A.J. 2007. Direct numerical simulation of flow in spacer-filled channels: Effect of spacer geometrical characteristics. Journal of Membrane Science 291(1), 53-69.

Koutsou, C.P., Yiantsios, S.G. and Karabelas, A.J. 2009. A numerical and experimental study of mass transfer in spacer-filled channels: Effects of spacer geometrical characteristics and Schmidt number. Journal of Membrane Science 326(1), 234-251.

Lecuyer, S., Rusconi, R., Shen, Y., Forsyth, A., Vlamakis, H., Kolter, R. and Stone, H.A. 2011. Shear stress increases the residence time of adhesion of Pseudomonas aeruginosa. Biophysical Journal 100(2), 341-350.

Li, Y.-L., Tung, K.-L., Chen, Y.-S. and Hwang, K.-J. 2012. CFD analysis of the initial stages of particle deposition in spiral-wound membrane modules. Desalination 287, 200-208.

Liu, Y. and Tay, J.-H. 2002. The essential role of hydrodynamic shear force in the formation of biofilm and granular sludge. Water Research 36(7), 1653-1665.

Neal, P.R., Li, H., Fane, A.G. and Wiley, D.E. 2003. The effect of filament orientation on critical flux and particle deposition in spacer-filled channels. Journal of Membrane Science 214(2), 165-178.

Journal Pre-proof

Pang, C.M., Hong, P., Guo, H. and Liu, W.-T. 2005. Biofilm formation characteristics of bacterial isolates retrieved from a reverse osmosis membrane. Environmental Science & Technology 39(19), 7541-7550.

Perni, S., Jordan, S.J., Andrew, P.W. and Shama, G. 2006. Biofilm development by Listeria innocua in turbulent flow regimes. Food Control 17(11), 875-883.

Persat, A., Stone, H.A. and Gitai, Z. 2014. The curved shape of Caulobacter crescentus enhances surface colonization in flow. Nature Communications 5(1), 3824.

Purevdorj, B., Costerton, J.W. and Stoodley, P. 2002. Influence of hydrodynamics and cell signaling on the structure and behavior of Pseudomonas aeruginosa biofilms. Applied and Environmental Microbiology 68(9), 4457-4464.

Qamar, A., Bucs, S., Picioreanu, C., Vrouwenvelder, J. and Ghaffour, N. 2019. Hydrodynamic flow transition dynamics in a spacer filled filtration channel using direct numerical simulation. Journal of Membrane Science 590, 117264.

Qamar, A., Samtaney, R. and Bull, J.L. 2012. Pulsatility role in cylinder flow dynamics at low Reynolds number. Physics of Fluids 24(8), 081701.

Radu, A.I., van Steen, M.S.H., Vrouwenvelder, J.S., van Loosdrecht, M.C.M. and Picioreanu, C. 2014. Spacer geometry and particle deposition in spiral wound membrane feed channels. Water Research 64, 160-176.

Radu, A.I., Vrouwenvelder, J.S., van Loosdrecht, M.C.M. and Picioreanu, C. 2010. Modeling the effect of biofilm formation on reverse osmosis performance: Flux, feed channel pressure drop and solute passage. Journal of Membrane Science 365(1), 1-15.

Journal Pre-proof

Radu, A.I., Vrouwenvelder, J.S., van Loosdrecht, M.C.M. and Picioreanu, C. 2012. Effect of flow velocity, substrate concentration and hydraulic cleaning on biofouling of reverse osmosis feed channels. Chemical Engineering Journal 188, 30-39.

Rickard, A.H., McBain, A.J., Stead, A.T. and Gilbert, P. 2004. Shear rate moderates community diversity in freshwater biofilms. Applied and Environmental Microbiology 70(12), 7426-7435.

Roosjen, A., Boks, N.P., van der Mei, H.C., Busscher, H.J. and Norde, W. 2005. Influence of shear on microbial adhesion to PEO-brushes and glass by convective-diffusion and sedimentation in a parallel plate flow chamber. Colloids and Surfaces B: Biointerfaces 46(1), 1-6.

Sanawar, H., Bucs, S.S., Pot, M.A., Zlopasa, J., Farhat, N.M., Witkamp, G.-J., Kruithof, J.C., van Loosdrecht, M.C.M. and Vrouwenvelder, J.S. 2019. Pilot-Scale Assessment of Urea as a Chemical Cleaning Agent for Biofouling Control in Spiral-Wound Reverse Osmosis Membrane Elements. Membranes 9(9), 117.

Saur, T., Morin, E., Habouzit, F., Bernet, N. and Escudié, R. 2017. Impact of wall shear stress on initial bacterial adhesion in rotating annular reactor. PLOS ONE 12(2), e0172113.

Schock, G. and Miquel, A. 1987. Mass transfer and pressure loss in spiral wound modules. Desalination 64, 339-352.

Schwinge, J., Neal, P.R., Wiley, D.E., Fletcher, D.F. and Fane, A.G. 2004a. Spiral wound modules and spacers: Review and analysis. Journal of Membrane Science 242(1), 129-153.

Schwinge, J., Wiley, D.E. and Fane, A.G. 2004b. Novel spacer design improves observed flux. Journal of Membrane Science 229(1), 53-61.

Schwinge, J., Wiley, D.E., Fane, A.G. and Guenther, R. 2000. Characterization of a zigzag spacer for ultrafiltration. Journal of Membrane Science 172(1), 19-31.

Schwinge, J., Wiley, D.E. and Fletcher, D.F. 2002a. Simulation of the flow around spacer filaments between channel walls. 2. Mass-transfer enhancement. Industrial & Engineering Chemistry Research 41(19), 4879-4888.

Schwinge, J., Wiley, D.E. and Fletcher, D.F. 2002b. Simulation of the flow around spacer filaments between narrow channel walls. 1. Hydrodynamics. Industrial & Engineering Chemistry Research 41(12), 2977-2987.

Shen, Y., Monroy, G.L., Derlon, N., Janjaroen, D., Huang, C., Morgenroth, E., Boppart, S.A., Ashbolt, N.J., Liu, W.-T. and Nguyen, T.H. 2015. Role of biofilm roughness and hydrodynamic conditions in Legionella pneumophila adhesion to and detachment from simulated drinking water biofilms. Environmental Science & Technology 49(7), 4274-4282.

Siddiqui, A., Farhat, N., Bucs, S.S., Linares, R.V., Picioreanu, C., Kruithof, J.C., van Loosdrecht, M.C.M., Kidwell, J. and Vrouwenvelder, J.S. 2016. Development and characterization of 3D-printed feed spacers for spiral wound membrane systems. Water Research 91, 55-67.

Siddiqui, A., Lehmann, S., Bucs, S.S., Fresquet, M., Fel, L., Prest, E.I.E.C., Ogier, J., Schellenberg, C., van Loosdrecht, M.C.M., Kruithof, J.C. and Vrouwenvelder, J.S. 2017. Predicting the impact of feed spacer modification on biofouling by hydraulic characterization and biofouling studies in membrane fouling simulators. Water Research 110, 281-287.

Journal Pre-proof

Siddiqui, S., Chandrasekaran, A., Lin, N., Tufenkji, N. and Moraes, C. 2019. Microfluidic shear assay to distinguish between bacterial adhesion and attachment strength on stiffness-tunable silicone substrates. Langmuir 35(26), 8840-8849.

Sreedhar, N., Thomas, N., Al-Ketan, O., Rowshan, R., Hernandez, H., Abu Al-Rub, R.K. and Arafat, H.A. 2018. 3D printed feed spacers based on triply periodic minimal surfaces for flux enhancement and biofouling mitigation in RO and UF. Desalination 425, 12-21.

Subramani, A. and Hoek, E.M.V. 2008. Direct observation of initial microbial deposition onto reverse osmosis and nanofiltration membranes. Journal of Membrane Science 319(1), 111-125.

Tritton, D.J. 2012. Physical Fluid Dynamics. Science.

Vrijenhoek, E.M., Hong, S. and Elimelech, M. 2001. Influence of membrane surface properties on initial rate of colloidal fouling of reverse osmosis and nanofiltration membranes. Journal of Membrane Science 188(1), 115-128.

Vrouwenvelder, J.S., Graf von der Schulenburg, D.A., Kruithof, J.C., Johns, M.L. and van Loosdrecht, M.C.M. 2009a. Biofouling of spiral-wound nanofiltration and reverse osmosis membranes: A feed spacer problem. Water Research 43(3), 583-594.

Vrouwenvelder, J.S., Hinrichs, C., Van der Meer, W.G.J., Van Loosdrecht, M.C.M. and Kruithof, J.C. 2009b. Pressure drop increase by biofilm accumulation in spiral wound RO and NF membrane systems: role of substrate concentration, flow velocity, substrate load and flow direction. Biofouling 25(6), 543-555.

Ying, W., Gitis, V., Lee, J. and Herzberg, M. 2013. Effects of shear rate on biofouling of reverse osmosis membrane during tertiary wastewater desalination. Journal of Membrane Science 427, 390-398.

Journal Pre-proof

Zimmerer, C.C. and Kottke, V. 1996. Effects of spacer geometry on pressure drop, mass transfer, mixing behavior, and residence time distribution. Desalination 104(1), 129-134.

Declaration of interests

☒ The authors declare that they have no known competing financial interests or personal relationships that could have appeared to influence the work reported in this paper.

TOC

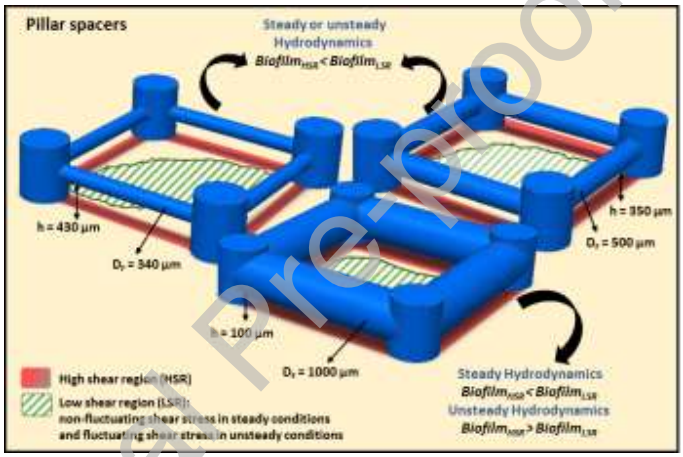

Journal Pre-proof